Electrodynamics of nanoantenna-mom diode infrared sensors

Gábor Matyi

Advisor:

Dr. Árpád Csurgay
Member of MTA

Budapest 2007

Készült
a Pázmány Péter Katolikus Egyetem
Információs Technológia Kar
Interdiszciplináris Mûszaki Tudományok
Doktori Iskola
keretében,

a Magyar Tudományos Akadémia
Számítástechnikai és Automatizálási Kutató
Intézet
Analogikai és Neurális Számítások
Laboratórium
támogatásával

I. Introduction

Infrared imaging systems were already built since the 60's. These sensor needs cryogenic temperature during their operation. The next step was the developing the uncooled bolometric infrared sensors in the 80's ([1]-[4]).
The nanoantenna mom diode system has been examined since 70's ([10]). This type of sensor has a CMOS compatible technology; it can theoretically operate in different frequency bands, and doesn't need cryogenic temperature during operation. During the last few decades it was widely investigated ([5]-[10]). In these works the nanoantenna mom diode system was only experimentally investigated with spiral, bow tie and dipole antennas.
On the basis of ([5]-[10]) the classical electrodynamics can be used in modeling the nanoantenna mom diode system. Although these papers contains many experimentally results, and they prove that the nanoantenna mom diode system is a frequency selective sensor they don't want to built double band on chip integrated sensor.
By using the classical electrodynamics, the nanoantenna mom diode system can be investigated in a deeper theoretical way. By using the classical electrodynamics we can easily modify the geometry of the nanoantenna mom sensor in order to build a double band sensor which is compatible with the high capacity CMOS electronics.
We have to use a robust numerical electromagnetic analyzing method (TLM) in order to reliably model the electromagnetic field around the sensor. The TLM method was already successfully used in the analysis of the classical electromagnetic problems ([12]) and in the analysis of the infrared filters ([12]-[13]). During the simulations I used the MicroStripes software of the Flomerics Inc [12]. In the common literature there are many papers about the theoretical background of the TLM method ([12]-[13]). They don't give a rigorous derivation of the TLM method.
Although the nanoantenna mom diode system has a very low sensitivity ([5]-[10]), there are no method by which the sensitivity can significantly increased.

II. A feladat során alkalmazott módszerek rövid elemzése

We have to use the classical electrodynamics [18],[19] for the modeling of the electromagnetic field around the nanoantenna mom diode sensor. In the [18],[19] the electromagnetic field of cavities, antennas and waveguides is described. These works are based on the Maxwell equations.

We directly use the classical antenna theory during the modeling of the antenna-mom infrared sensors. Detailed models for different antenna types and detailed descriptions of the behavior of antennas are described in [20].

The geometry of the nanoantenna mom diode system is very similar to the microstrip antennas we focused on the theory of the microstrip antennas. Detailed theory and experimental results of microstrip antennas are given in [21]. In this work a general and detailed review is given about the theory of the microstrip antennas, about the applications of the microstrip antennas, about the design considerations of the microstrip antennas and about the geometry of the microstrip antennas.

Besides of the antenna theory we have to use numerical methods during the analyzis of the sensor. I used the TLM method based MicroStripes software (Flomerics Inc). The TLM method is based on the combination of the waveguide theory and the finite difference method [14]-[17]. I studied the theory of the electromagnetic field in waveguides [22], [23]-[25] Besides [14]-[17]. The [22], [23]-[25] works are based on the Maxwell equations and using the Marcuwitz Schwinger equations in order to model the electromagnetic field in waveguides.

We have to study the model by which we can describe the interaction between the electromagnetic field and matter. We have to accurately modeling this interaction because our sensor is operates in the infrared regime in order to adequately model our sensor. The interaction between dielectrics metals and the electromagnetic field is accurately described in [26]-[29] (experimentally and theoretically). We have to study the quantum theory [30] in order to deeply understand the theoretical background of the interaction of the field and matter.

III. Thesis

1. I showed that the TLM matrix can be derived by using the Marcuwitz-Schwinger equations by using harmonic signals in the presence of isotropic, homogenous, time invariant, lossless medium.

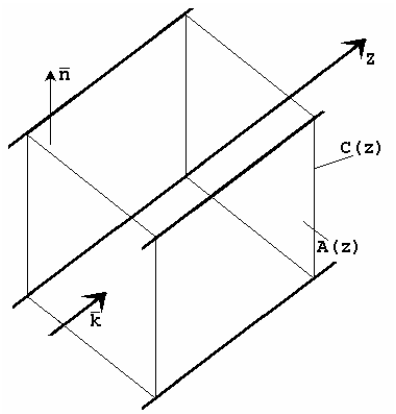

1. Figure The geometry of a rectangular waveguide

The equations (1) are called as the Marcuwitz-Schwinger equations.

$$\begin{aligned} -\frac{\partial U_i}{\partial z} &= Z_i I_i - P_i - P_{ij} \\ -\frac{\partial I_i}{\partial z} &= Y_i U_i - Q_i - Q_{ij} \end{aligned}, \tag{1}$$

where

$$Y_i = \begin{cases} j\omega\varepsilon & \text{for TEM and TE} \\ j\omega\varepsilon + \dfrac{k_i^2}{j\omega\mu} & \text{for TM} \end{cases}, \tag{2}$$

$$Z_i = \begin{cases} j\omega\mu & \text{for TEM and TM} \\ j\omega\mu + \dfrac{k_i^2}{j\omega\varepsilon} & \text{for TE} \end{cases}, \tag{3}$$

$$P_i = \frac{1}{j\omega\mu}\oint_C \left(\bar{E}_t \times \bar{n}\right)\left(\bar{\nabla}_t \times \bar{e}_i\right) dl, \tag{4}$$

$$P_{ij} = \int_A \bar{e}_i \bar{J}_t dA, \tag{5}$$

$$Q_i = \oint_C E_z \bar{e}_i * \bar{n} dl, \tag{6}$$

$$Q_{ij} = \frac{1}{j\omega\varepsilon}\int_A \bar{e}_i \bar{\nabla}_t J_z dA. \tag{7}$$

$A(z)$ is the cross sectional area of the waveguide (Fig.1.) and $C(z)$ is the contour of $A(z)$. The electromagnetic field inside the waveguide can be decomposed into transversal and longitudinal components. The longitudinal component can be calculated from the transversal components. The transversal components can be represented by a modal series where $\bar{e}_i$ and

$\bar{h}_i$ are orthonormal vectorial eigenfunctions of the i-th mode. The U_i and I_i are the modal voltage and modal current of the i-th mode and they are functions of z

$$\begin{aligned} \bar{E}_t &= \sum_i \bar{e}_i U_i \\ \bar{H}_t &= \sum_i \bar{h}_i I_i . \end{aligned} \qquad (8)$$

Equations (1-6) give us the generalized transmission line model for the arbitrarily cross section waveguide. By using the modal expansion of the field components (8) the partial differential Maxwell equations can be decomposed to infinite ordinary equations. Equations (1-6) are powerful tool in modeling waveguide structures under several geometrical and material properties.

Derivation of the TLM matrix

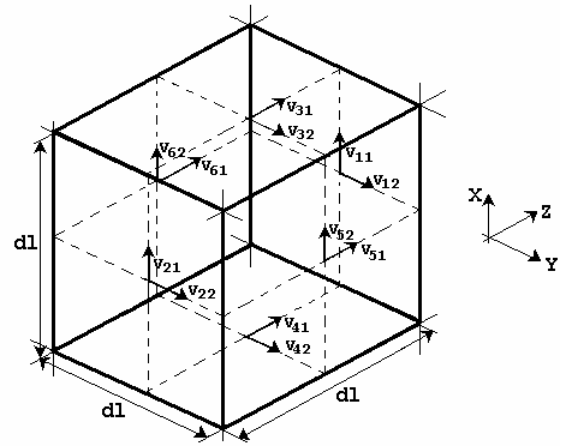

2. Figure The TLM cell

Now we derive the scattering matrix of the TLM cell (Fig.2.) by using the Marcuwitz-Schwinger equations. We assume for the simplicity that the whole volume is filled by vacuum (there are no electric currents in the volume). We assume further that the field variation on the surface of the TLM cell is small enough to be neglected. In this case the field on the surface can be described by two orthogonal TEM modes (signed by V_{i1}, V_{i2} on Fig.2.).

The TLM cell can be represented as the cross of three rectangular waveguide. The three waveguides are directed to the ‘ x ’, ‘ y ’ and ‘ z ’.

For example in the ‘ z ’ directed waveguide there are two TEM modes: one is directed to ‘ x ’ and propagates into ‘ z ’. Its vectorial eigenfunction is

$$\bar{e}_{zx} = \left\{ \frac{1}{\Delta l}, 0, 0 \right\}, \qquad (9)$$

and the other is directed to ‘ y ’ and propagates into ‘ $-z$ ’. Its vectorial eigenfunction is

$$\bar{e}_{zy} = \left\{ 0, -\frac{1}{\Delta l}, 0 \right\}. \qquad (10)$$

We can similarly synthesize the eigenfunctions of the other two waveguides. The other two waveguides (the ‘ x ’, ‘ y ’ directed waveguide) and the TEM modes in these waveguides couple through the sides of the TLM cube to the ‘ z ’ waveguide. We want to describe this coupling effect between the different sides of the TLM cube. We consider the modal voltage amplitudes in the two opposite side of the TLM cell in the ‘ z ’ directed waveguide as (V_{11}, V_{12} and the other is V_{21}, V_{22}). The TEM modes in the ‘ x ’, ‘ y ’ directed waveguide operate in the ‘ z ’ waveguide as generators (through the integrals (4, 5)).

After substitution the integrals (4,5) to the Marcuwitz-Schwinger equations (1) and solving these equations for every TEM modes on the waveguides we can write the admittance matrix ($\underline{\underline{Y}}$) of the TLM cell in case of TEM modes between the modal voltages and modal currents

	V_{11}	V_{12}	V_{21}	V_{22}	V_{31}	V_{32}	V_{41}	V_{42}	V_{51}	V_{52}	V_{61}	V_{62}
I_{11}	a	0	b	0	c	0	c	0	0	0	0	0
I_{12}	0	a	0	b	0	0	0	0	c	0	c	0
I_{21}	b	0	a	0	c	0	c	0	0	0	0	0
I_{22}	0	b	0	a	0	0	0	0	c	0	c	0
I_{31}	c	0	c	0	a	0	b	0	0	0	0	0
I_{32}	0	0	0	0	0	a	0	b	0	c	0	c
I_{41}	c	0	c	0	b	0	a	0	0	0	0	0
I_{42}	0	0	0	0	0	b	0	a	0	c	0	c
I_{51}	0	c	0	c	0	0	0	0	a	0	b	0
I_{52}	0	0	0	0	0	c	0	c	0	a	0	b
I_{61}	0	c	0	c	0	0	0	0	b	0	a	0
I_{62}	0	0	0	0	0	c	0	c	0	b	0	a

Table1. The Admittance matrix ($\underline{\underline{Y}}$) of the TLM cell

where

$$a = -j\frac{\sqrt{\varepsilon}\,Cot(\sqrt{\varepsilon}\sqrt{\mu}\Delta l\omega)}{\sqrt{\mu}}, \tag{11}$$

$$b = -j\frac{\sqrt{\varepsilon}}{\sqrt{\mu}\,Sin(\sqrt{\varepsilon}\sqrt{\mu}\Delta l\omega)}, \tag{12}$$

$$c = -j\frac{1}{\Delta l\mu\omega}. \tag{13}$$

The admittance matrix has only imaginary values because there is no dissipation in the vacuum. The admitane matrix are symmetric and reciprocal. The $\underline{\underline{Y}}$ matrix can easily rewrite by using the scattering formalism

$$U_i = \sqrt{R_i}\left(a_i + b_i\right) \tag{14}$$

$$I_i = \frac{1}{\sqrt{R_i}}\left(a_i - b_i\right) \tag{15}$$

where R_i is the normalizing constant and a_i is the incident wave and b_i is the reflected wave. The scattering matrix

$$\underline{\underline{S}} = \left(\underline{\sqrt{R}}\,\underline{\underline{E}} - \underline{\underline{Y}}\right)\left(\underline{\sqrt{R}}\,\underline{\underline{E}} + \underline{\underline{Y}}\right)^{-1}$$

can be easily calculated from the admittance matrix, where $\underline{\underline{E}}$ is the unit matrix and $\underline{\sqrt{R}}$ is the vector of the normalizing constants.

2. I developed the equivalent circuit model for the double band nanoantenna-mom diode infrared sensor

A single band nanoantenna-mom diode sensor layout is shown on fig. 3-4. The infrared sensor is placed on the top of a CMOS chip. We place a thin dielectric layer between the top metal layer of the chip and the nanoantenna. A simple nanoantenna mom diode system is a nanoantenna separated by a tunnel diode and a low pass filter in order to suppress the THz frequency components.

The incoming infrared radiation generates currents in the antenna.These currents flow through the tunnel diode which rectifies the THz signal. The rectified DC signal can flow through the arms of the low pass filter. The bias point of the diode can be set through the arms of the low pass filter.

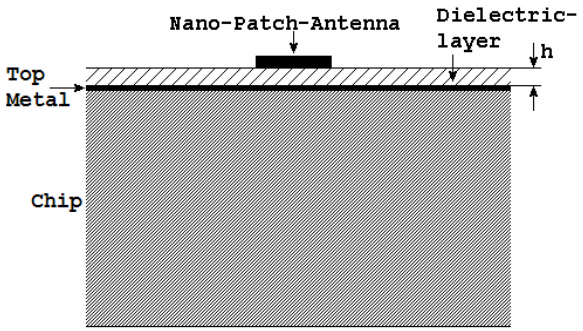

3. Figure The cross section of a single-band infrared sensor

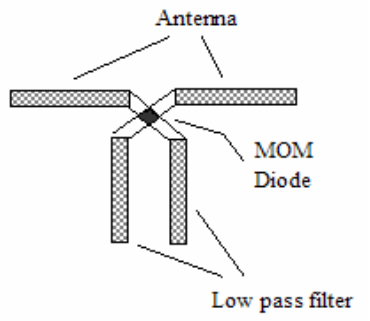

4. Figure The top view of a single-band infrared sensor [6]-[10].

The equivalent circuit model for single band naoantenna mom diode sensor is shown in fig. 5 [10]. The antenna (in receiving mode) can be modeled by a serial connected voltage generator and frequency dependent complex impedance ($Z_{ant} = R_A + jX_A$). The mom diode can be modeled by a parallel connected nonlinear resistor and capacity. The low pass filter is modeled by an ideal inductivity the bias circuit can be modeled by a resistivity and a DC voltage generator. The THz signal of the output can be seen in fig. 6.

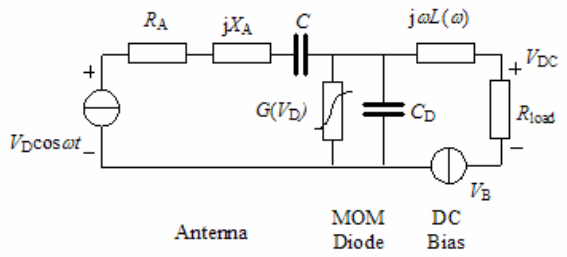

5. Figure Circuit model for single band infrared sensor [10]

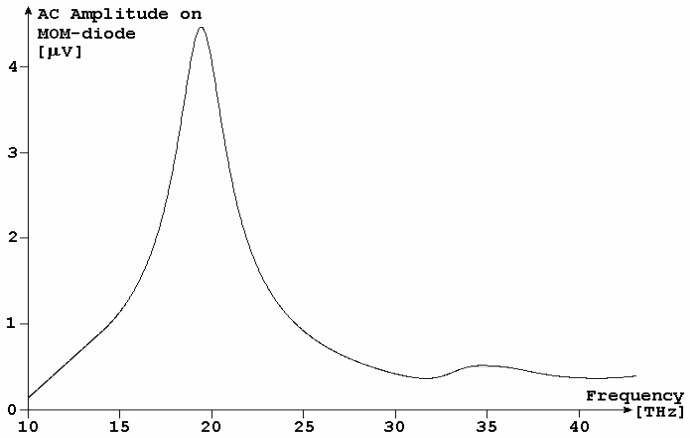

6. Figure Single band THz rectifier characteristics in frequency domain versus frequency

We can easily form a double band infrared sensor system by using two single band infrared sensors (fig. 7). By using the classical electrodynamics and classical antenna theory we can easily give an equivalent circuit model for the double band IR sensor (fig. 8).

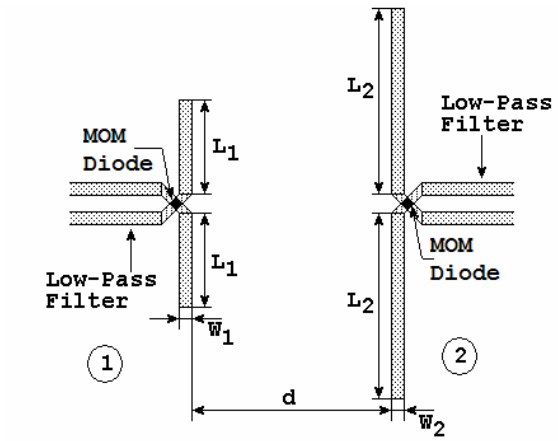

7. Figure The top view of a double-band infrared sensor

The nanoantenna system in receiving mode can be modeled by an equivalent linear circuit with three gates. Two gates are the outputs of the antennas and the third one models the incoming IR radiation (by a voltage generator). The linear system of the antennas can be modeled by an impedance matrix. On the outputs of the antennas we can connect the equivalent models for tunnel diode and bias circuit (fig. 8). The parameters of the equivalent impedance matrix can be determined by the TLM method [11].

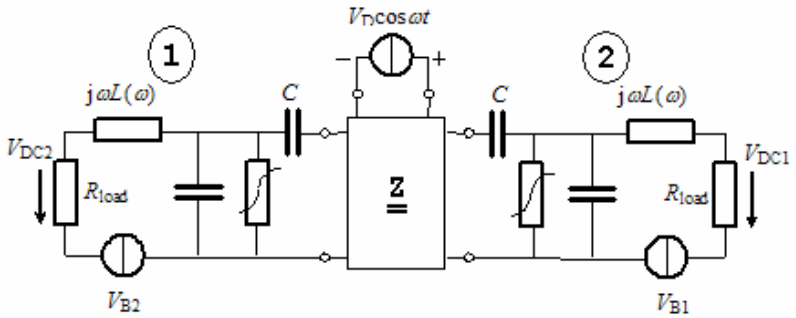

8. Figure Circuit model for double band infrared sensor

By analyzing the equivalent circuit model (on fig. 8) the THz signals on the outputs can easily be determined (fig. 9). On fig. 9 we can see that the signals on the outputs of the two antennas

are separated versus frequency. The double band system on fig. 7 can be used as a double band IR sensor.

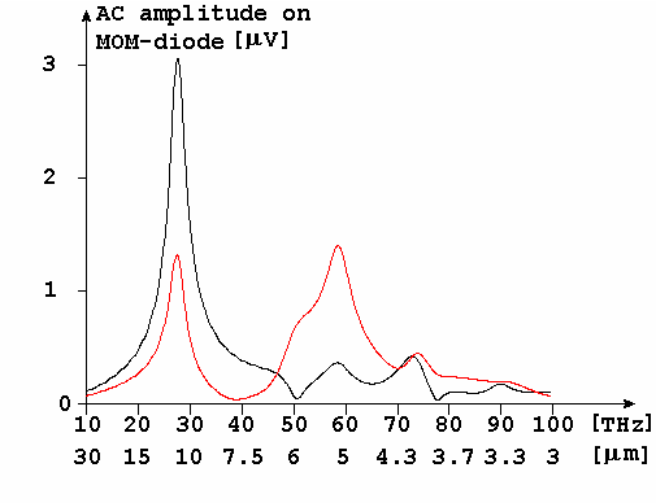

9. Figure Double band THz rectifier characteristics in frequency domain versus frequency (the black curve is related to the longer antenna the red curve is related to the shorter antenna

On fig 9 we can see that there is a strong crosstalk between the two antennas on the lower resonance frequency. By varying the relative positions of the antennas (fig. 10) the crosstalk between the antennas ca be significantly suppress (fig. 11).

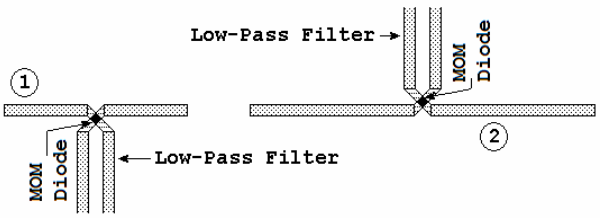

10. Figure A possible layout for double band infrared sensor

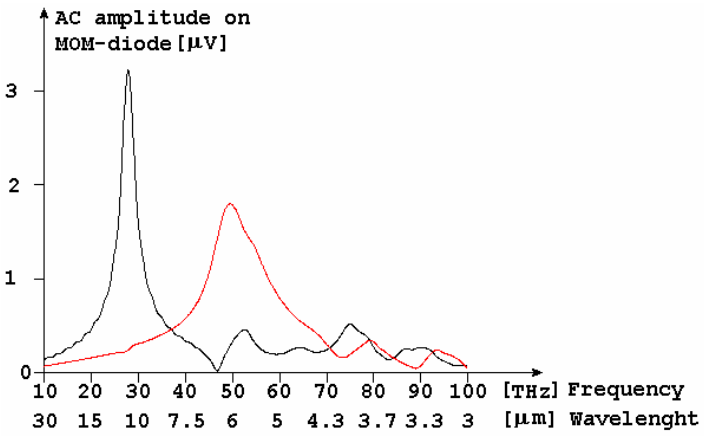

11. Figure Double band THz rectifier characteristics in frequency domain versus frequency (the black curve is related to the longer antenna the red curve is related to the shorter antenna

On figures 6, 9, 11 we can see that the peak values of the received THz signal is $U_{AC} \approx 5mV$. The effective area ([20]) of the antenna can be calculated by using

$$A_{eff\ antenna} = \frac{P_{ACout}}{S_{in}}. \qquad (1)$$

where P_{ACout} is the AC power on the output of the antenna and $S_{in}\left[\frac{W}{m^2}\right]$ is the power density of the incoming radiation

$$S_{in} = \frac{\left|\overline{E}_{in}\right|^2}{Z_0}, \tag{2}$$

where $\overline{E}_{in}$ is the absolute value of the vector of the incoming electric field, Z_0 is the impedance of the vacuum (we assume that $\overline{E}_{in} = 2\left[\frac{V}{m}\right]$).

$$P_{ACout} = \frac{(U_{AC})^2}{R_D}, \tag{3}$$

where R_D is the resistance of the mom diode. In the furthers we assume that the DC and AC resistivity of the diode is equivalent ($R_D \approx 100\Omega$). By using the expressions above the equivalent area of the antenna is

$$A_{eff\ antenna} \approx 15\left[\mathrm{m}m^2\right]. \tag{4}$$

3. I developed a design method in order to increase the sensivity of the double band nanoantenna mom diode infrared sensor

The sensitivity of a rectifier depends on the effective aperture of the antenna (A_{eff}) [20]. However, A_{eff} strongly depends on the thickness of the dielectric-layer (Fig. 12) and the width of the antenna [21]. At small dielectric-layer thicknesses the A_{eff} is small. By increasing the thickness of the dielectric layer the A_{eff} increases until it reaches its optimal value. When we further increase the thickness the A_{eff} will decrease because more and more surface waves are generating on the border of the dielectric layer and it degrades A_{eff}. By increasing the width of the antenna we can further increase the value of A_{eff}.

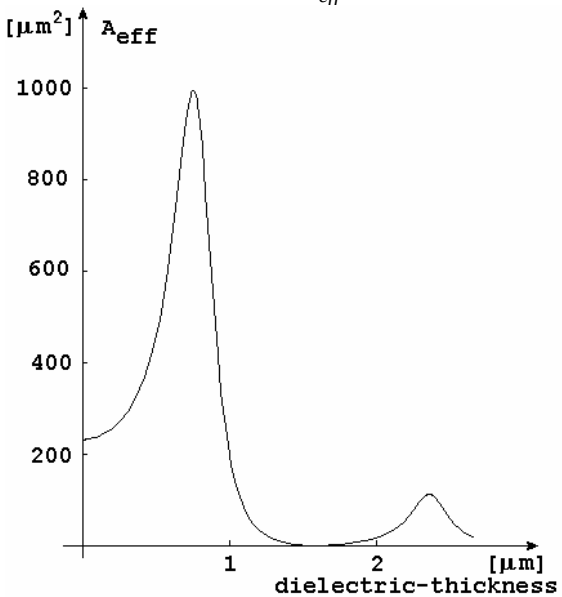

12. Figure The effective area of a nanoscale patch-antenna versus dielectric-layer t hickness (The other parameters are constant) based on [21]

The proposed design method in case of the single-band THz rectifier is illustrated on Fig.. 13. First, the initial, effective-length, $L_{e,}$ of the antenna is determined from the given frequency f_0. Next, the height of the dielectric-layer is looked for in order to make A_{eff} a maximum. Then, the geometrical length L of the antenna is determined from L_e and h. We can further increase A_{eff} by increasing the width W of the antenna.

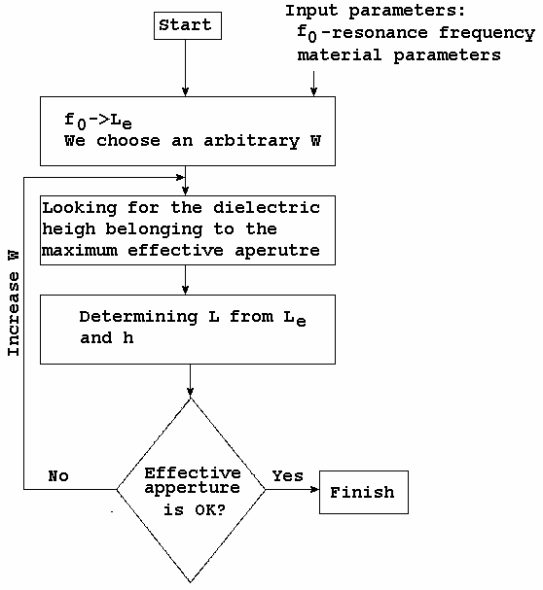

13. Figure The design algorithm for single band THz rectifier

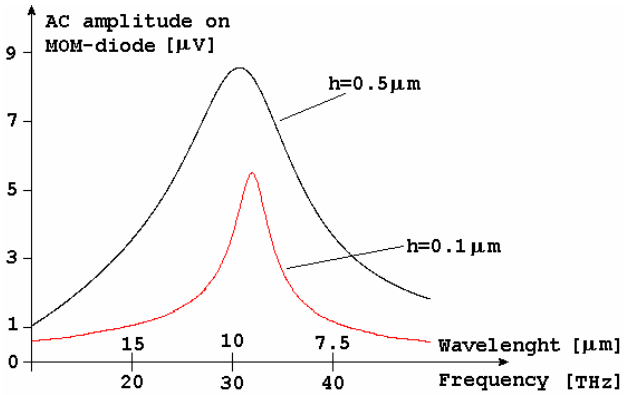

14. Figure Single band THz rectifier characteristics in frequency domain versus dielectric-layer thickness

For the double band case we have two antennas, and by applying the above design procedure to the two antennas we have two optimal dielectric-layer thicknesses for the two antennas. A thicker dielectric-layer is for the longer antenna and a thinner dielectric-layer for the shorter antenna. If we choose the thicker dielectric-layer, it is optimal for the longer antenna, but there will be strong surface wave excitation for the shorter antenna. Although the thinner dielectric-layer is not optimal for the longer antenna but there will be no strong surface wave excitation for the shorter- and longer-antenna. The thinner dielectric-layer turns to the optimal for the double-band case.

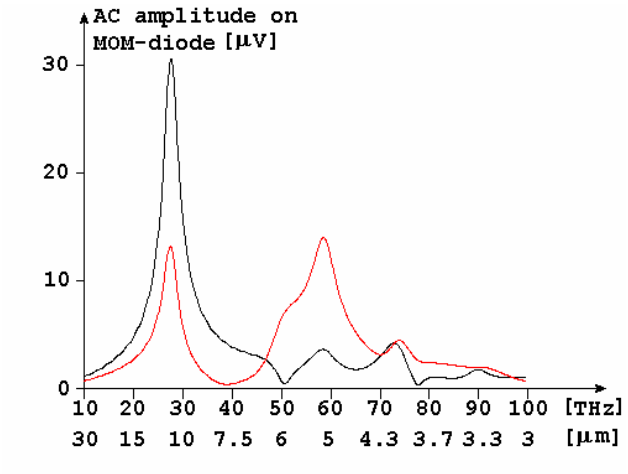

15. Figure Double band THz rectifier characteristics in frequency domain versus frequency after optimization (the black curve is related to the longer antenna the red curve is related to the shorter antenna

The optimization process above was done in the double band case. After the analysis of the optimized system the THz signal on the outputs of the antennas can be seen on fig. 15. The maximum values of the received THz signals are increased (comparing fig 15 with fig. 11).

4. I modified the geometry of the double band infrared sensor in order to increase the sensitivity

The effective aperture can be increased by using a large spherical dielectric lens above the MOM-nanoantenna system to focus the incident waves to the antenna (Fig. 16). The dielectric lens and the dielectric cylinder are assumed to be made of. The spherical dielectric lens focuses the incoming radiation to its focal point. We could put the nanoantenna to the focal point of the lens and we may use a silicon cylinder in order to hold the focal length between the dielectric lens and the nanoantenna. The lens collects the incoming radiations from a much greater aperture and focuses it to the antenna. Fig. 17 shows the estimated AC amplitude on the MOM diode of a nanoantenna THz rectifier in the frequency domain with a spherical dielectric lens.

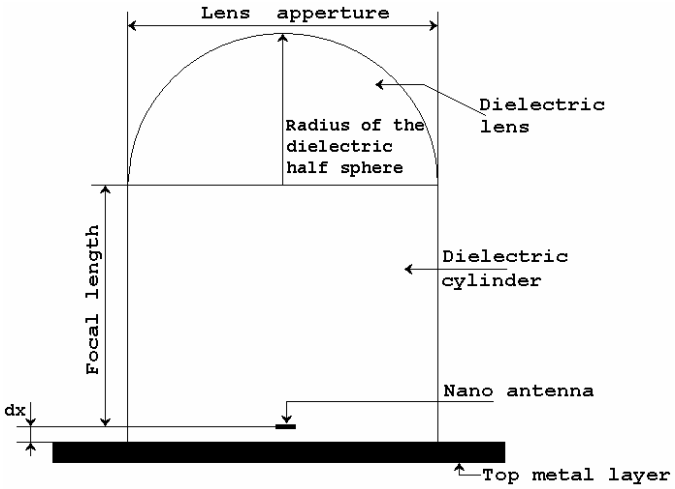

16. Figure Cross section of the single band dielectric lens infrared sensor

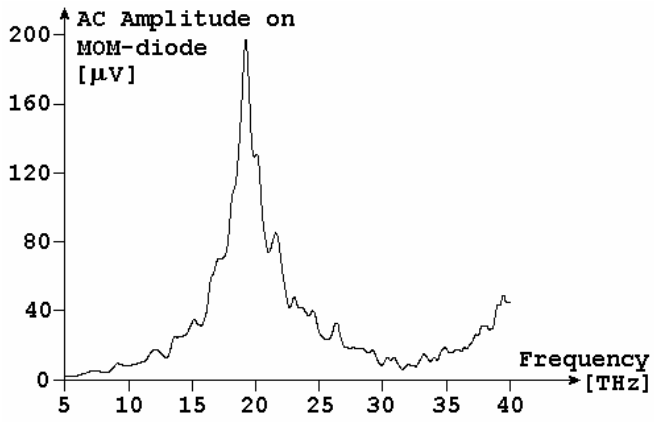

17. Figure The AC signal on the output of the antenna of the single band dielectric lens infrared sensor (aperture of the lens $40mm$)

Comparing Fig. 6 and Fig. 17 it can be stated that we can achieve relative amplification in AC amplitude (~60 times in this case) by using dielectric spherical lens. It can be read from Fig. 17 that the maximum of the amplitude of the THz signal is around $U_{AC} \approx 200mV$.

In order to get a double-band sensor, the single-band case geometry (Fig. 16) can be modified easily by putting the two antennas symmetrically around the focal point of the lens (Fig. 18). Complete EM analysis was done for the double-band dielectric lens cylinder structure in case of incident plane wave from z direction. This is plotted on Fig. 19. Although neither of the antennas are on the focal point of the lens the amplification is significant. The design procedure is the same above. The aperture size of the lens can be increased until both of the received signals reach the desired level on the MOM diode.

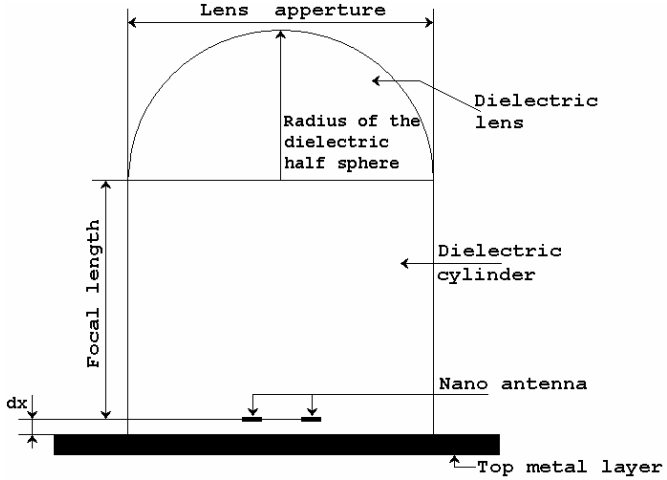

18. Figure Cross section of the double band dielectric lens infrared sensor

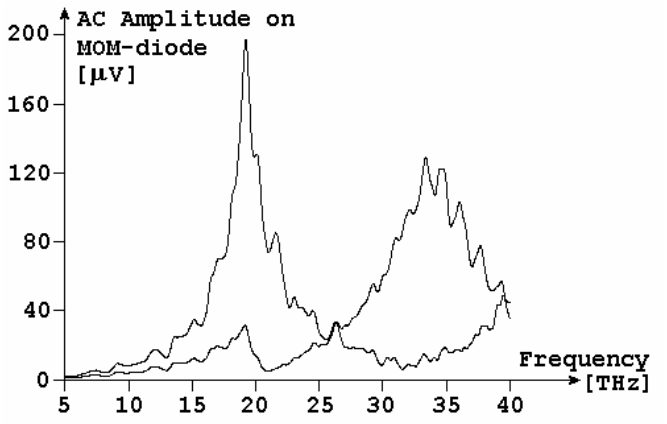

19. Figure The AC signal on the outputs of the two antennas of the double band dielectric lens infrared sensor (aperture of the lens $40mm$)

IV. Applications

Infrared sensors and infrared focal plane arrays had been already used [2] in many applications. Infrared sensors are widely used in surveillance, fire security, military and police applications.

The uncooled double band IR sensor has many advantages compared to the ordinary bolometric sensors. The uncooled nanoantenna-mom sensor is CMOS compatible, and it has high speed capability. Because of these abilities this type of sensors can be used more flexible and it has many new applications than the bolometric one (for example the medical applications) [31],[32].

V. Authors Papers

Gábor Matyi, “Nanonatennas for uncooled, double-band, CMOS compatibla, high-speed infrared sensors,” International Journal of Circuit Theory and Applications, vol.. 32, September-October. 2004, pp. 425-430

Gábor Matyi, “The TLM method and the Marcuwitz-Schwinger Equations,” in Proc. Mediterranean Microwave Symposium, Budapest, 2007 pp.

Gábor Matyi, Arpad I. Csurgay, Wolfgang Porod “Nanoantenna Design for THz-band Rectification”, in Proc. MWSCAS, August 2006,San Huan Puerto Rico

Gábor Matyi, “Dielectric Lens Nanoantennas for Uncooled, CMOS compatible, High Speed Double-band Infrared Sensors ” (Publikálás alatt)

VI. Bibliography

[1] A. Rogalski, Infrared detectors: an overview, Infrared Physics and Technology, 43 (2002) 187–210

[2] P. W. Kruse, D.D. Skatrud, Uncooled Infrared Imaging Arrays and Systems, Academic Press, 1997

[3] S. Eminoglu, D. S. Tezcan, M. Y. Tanrikulu, T. Akin, Low-cost uncooled infrared detectors in CMOS process, Sensors and Actuators A 109 (2003) 102–113

[4] S. V. Bandara, et. al, Four-band quantum well infrared photodetector array, Infrared Physics and Technology, 44 (2003) 369–375

[5] S. Y. Wang, T. Izawa, T. K. Gustafson, Coupling characteristics of thin-film metal–oxide–metal diodes at 10.6 μm, Appl. Phys. Lett. 27 (1975) 275–279

[6] I. Wilke, Y. Opplinger, W. Herrmann, F. K. Kneubühl, Nanometer Thin Film Ni–NiO–Ni Diodes for 30 THz Radiation, Appl. Phys. Q 58 (1994) 329–341

[7] C. Fumeaux, W. Herrmann, K. K. Kneubuhl, H. Rothuizen, Nanometer thin-film Ni–NiO–Ni diodes for detection and mixing of 30 THz radiation, Infrared Physics and Technology, 39 (1998) 123–183

[8] C. Fumeaux, J. Alda, G. D. Boreman, Lithographic antennas at visible frequencies, Optics Letters, 24 (1999) 1629–1631

[9] I. Codreanu, F. J. Gonzalez, G. D. Boreman, Detection mechanisms in microstrip dipole antenna-coupled infrared detectors, Infrared Physics and Technology, 44 (2003) 155–163

[10] A. Sanchez, C. F. Davis, Jr., K. C. Liu, A Javan, The MOM tunneling diode: Theoretical estimate of its performance at microwave and infrared frequencies, J. Appl. Phys. 49 (1978), 5270

[11] http://www.flomerics.com

[12] K. D. Möller, O. Steinberg, H. Grebel, Philippe Lalanne, “Thick inductive cross shaped metal meshes” Journal of Applied Physics., vol. 91, no. 12, pp.9461-9465, June 2002.

[13] Howard A. Smith, M. Rebbert, O. Steinberg, “Designer Infrared filters using stacked metal lattices” Applied Physics Letters, vol. 82, no. 21, pp. 3605-3607, May 2003.

[14] Hang Jin, Rüdiger Vahldieck, „Direct Derivations of TLM Symmetrical Condensed Node and Hybrid Symmetrical Condensed Node from Maxwell’s

Equations Using Centered Differencing and Averaging", IEEE Transaction on Microwave Theory and Techniques, Vol.42, No.12, December 1994, pp. 2554-2561

[15] P.B Johns, R. L. Beurle, „Numerical Solution of 2-dimensional scattering problems using a Transmission-line Matrix", Proc. IEE, Vol.118, No.9, September 1971, pp. 1203-1208

[16] John Paul, Christos Christopulos, David W. P. Thomas, „Generalized Material Models in TLM-Part 1: Materials with Frequency-Dependent Properties", IEEE Trans. Ant. Prop., Vol.47, No.10, Oct. 1999, pp. 1528-1534

[17] John Paul, Christos Christopulos, David W. P. Thomas, „Generalized Material Models in TLM-Part 2: Materials with Anisotropic Properties", IEEE Trans. Ant. Prop., Vol.47, No.10, Oct. 1999, pp. 1535-1542

[18] Simonyi Károly, Zombory László, Elméleti Villamosságtan, Mûszaki könvkiadó, Budapest, 2000

[19] Roger F. Harington Time-Harmonic Electromagnetic Fields 2001 IEEE Press, Wiley Interscience

[20] C. A. Balanis, Antenna Theory, John Wiley and Sons, 1997

[21] Kai Fong Lee, Wei Chen, Advances in microstrip and printed antennas, John wiley & sons, Inc. 1997, Ch. 5.

[22] Csurgay Árpád, Markó Szilárd, Mikrohullámú Passzív hálózatok, BME Mérnök Továbbképzõ Intézet 1965

[23] N. Marcuwitz, J. Schwinger, "On the Representation of the Electric and Magnetic Fields Produced by Currents and Discontinuities in Wave Guides" Journal of Applied Physics, vol. 22, no. 6, pp. 806-819, June 1951.

[24] H. J. Butterweck, "Über die Anregung elektromagnetischer Wellenleiter" A. E. Ü., vol. 16, no. 10, pp. 498-514, March 1962.

[25] C. G. Montgomery, R. H. Dicke, E. M. Purcell Principles of Microwave Circuits 1947

[26] M. Dressel and G. Grüner, Electrodynamics of Solids – Optical Properties of Electrons in Matter, Cambridge University Press, 2002

[27] H. Haug, Stephan W. Koch, Quantum Theory of the Optical and Electronical Proerties of Semiconductors 1990 World Scientific Publishing Co.

[28] Edward D. Palik, Handbook of Optical Constants of Solids, Academic Press, 1985

[29] M. A. Ordal, R. J. Bell, R. W. Alexander, Jr. L. L. Long, M. R. Querry, Optical Properties of Fourteen Metals in the infrared and far infrared: Al, Co, Au, Fe, Pb, Mo, Ni, Pd, Pt, Ag, Ti, V, and W, Applied Optics, 24 (1985) No.24, 4493–4498

[30] Csurgay Árpád, Simonyi Károly Az Információtechnika Fizikai Alapjai 1997 Mérnöktovábbképzõ Intézet

[31] Pareja-Illeras Rosario, Diaz-Caro Jose, Blanco-Bartolomé Carmen, Linares-Herrero Rodrigo, Ramos-Marín Joaquín, Ortiz Sergio, „Design and comparison of multi- and hyper- spectral imaging systems”, Proc. of SPIE Vol. 5987, (2005), pp.

[32] Mark Dombrowski, Jagmohan Bajaj, Paul Willson, „Video-rate Visible to LWIR Hyperspectral Imaging and Image Exploitation”, Proceedings of the 31st Applied Imagery Pattern Recognition Workshop, IEEE, 2002